ChemComm

Crystal Structure and Orientation of Organic Semiconductor Thin Films by Microcrystal Electron Diffraction and Grazing-Incidence Wide-angle X-ray Scattering

Journal:	*ChemComm*
Manuscript ID	CC-COM-01-2020-000119.R2
Article Type:	Communication

COMMUNICATION

Crystal Structure and Orientation of Organic Semiconductor Thin Films by Microcrystal Electron Diffraction and Grazing-Incidence Wide-angle X-ray Scattering

Received 00th January 20xx,
Accepted 00th January 20xx

DOI: 10.1039/x0xx00000x

Andrew M. Levine[a,b,c], Guanhong Bu[d,e], Sankarsan Biswas[a,b,c], Esther H. R. Tsai*[f], Adam B. Braunschweig*[a,b,c] , and Brent L. Nannenga*[d,e]

We use microcrystal electron diffraction (MicroED) to determine structures of three organic semiconductors, and show that these structures can be used along with grazing-incidence wide-angle X-ray scattering (GIWAXS) to understand crystal packing and orientation in thin films. Together these complimentary techniques provide unique structural insights into organic semiconductor thin films, a class of materials whose device properties and electronic behavior are sensitively dependent on solid-state order.

Organic semiconductor films are active components in a number of electronic devices, including organic field effect transistors (OFET)[1] and organic photovoltaics (OPV)[2], because they conduct electricity in response to charge injection or irradiation with light. The optoelectronic responses of these devices are sensitively dependent upon the packing geometry of the organic semiconductors in their active layers[3], so solving their crystal structure is essential for understanding and, ultimately, predicting device properties, such as charge transport mechanism, mobility, and conductance. Determination of molecular packing and orientation, however, can be challenging because of the difficulty in crystallizing samples with sufficient dimensions necessary (> $1x10^3$ μm^3) for conventional single crystal X-ray diffraction (XRD) techniques, and these data still do not provide information about crystallite orientation and alignment within the device active layer film. Therefore, there is a need for new methods for high-resolution structure determination that can be carried out on the small crystallites typically found in synthesized samples and a way for determining whether these same unit cell structures are prevalent in the thin films used in the active layers of devices.

Microcrystal electron diffraction (MicroED) is an emerging method for the collection of electron diffraction data from crystallites several orders of magnitude smaller than what is required for single crystal XRD experiments[4]. This method bypasses additional crystallization steps, which can often be difficult and time consuming, thereby facilitating rapid structure determination. Recently, MicroED has been extended to the study of small organic molecules from nanocrystalline powders[5], but this technique has still not been adopted widely for analyzing organic semiconductors. Here we apply MicroED for the structural determination of three organic semiconductors of the rylene and diketopyrrolopyrrole (DPP) classes. The molecules investigated are two rylene bisimides[6, 7] – dipyrrolodine perylene diimide (dPyr PDI)[8, 9] and dicyano naphthalene diimide (dCN NDI)[10] – and a diketopyrrolopyrrole (dDPP)[11], all of which have been explored previously in the context of organic optoelectronic devices. The successful determination of these three structures from unrefined powders demonstrates the facility with which this technique is applied to organic semiconductors and is therefore ideal for deriving structure-activity relationships in a class of compounds whose desirability is based upon properties that arise from the relative spatial arrangement in the solid state. Grazing-incidence wide-angle X-ray scattering (GIWAXS) was used to determine if the films and the crystals possess the same unit cell

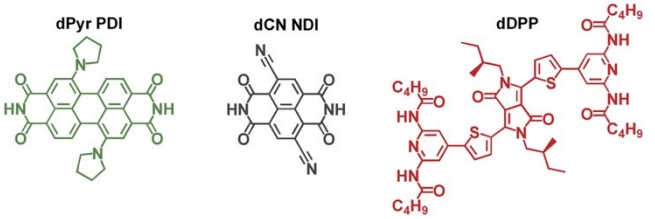

[a.] *Nanoscience Initiative, Advanced Science Research Center, Graduate Center, City University of New York, 85 St. Nicholas Terrace, New York, NY 10031, USA.*
[b.] *Department of Chemistry, Hunter College, 695 Park Avenue, New York, NY 10065, USA.*
[c.] *Ph.D. Program in Chemistry, The Graduate Center of the City University of New York, New York, NY 10016, USA.*
[d.] Chemical Engineering, School for Engineering of Matter, Transport, and Energy, Arizona State University, Tempe, AZ 85287, USA.
[e.] *Center for Applied Structural Discovery, The Biodesign Institute, Arizona State University, Tempe, AZ 85287, USA.*
[f.] Center for Functional Nanomaterials, Brookhaven National Laboratory, Upton, NY 11973, USA.
† Footnotes relating to the title and/or authors should appear here.
Electronic Supplementary Information (ESI) available: Procedures and details of synthesis, sample preparation, data collection, data processing, and crystallographic information. CCDC 1963919, 1963921, and 1963922 for dPyr PDI, dCN NDI, and dDPP, respectively. See DOI: 10.1039/x0xx00000x

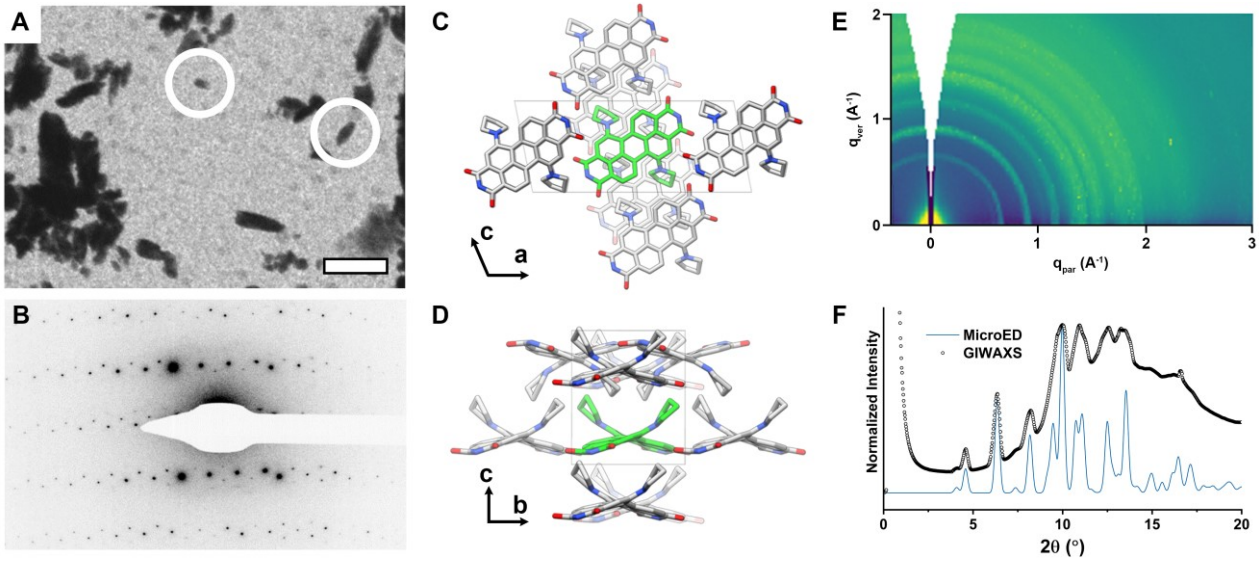

Fig. 1. Determination of dPyr PDI structure and film packing. (A) TEM micrograph of dPyr PDI crystallites with circles indicating particles selected for further analysis. Scale bar is 2 µm. (B) MicroED diffraction pattern of dPyr PDI crystallites extending to 0.60 Å. (C, D) Unit cell (box) of solved crystal structure with asymmetric Cc space group packing, single molecule of dPyr PDI shown in green. Pyrrolidine substituents on adjacent molecules form an alternating π-stacked structure where dPyr PDI molecular planes are 6.74 Å apart when separated by pyrrolidine groups and 4.01 Å when not. Atom colors: C, grey; N, blue; O, red. H have been omitted for clarity. (E) GIWAXS scattering pattern of dPyr PDI drop-casted thin film on glass slide shows no preferred orientation with respect to the substrate. (F) Overlay of GIWAXS 1D integrated intensity (black) and CrystalDiffract simulated powder pattern (blue) generated from MicroED determined unit cell.

and also add detail such as packing orientation with respect to the substrate. Together, these techniques offer a full picture of how organic semiconductors organize in thin films, and this work is a model for how a more complete understanding of organic thin film behavior can be achieved.

The first sample we analyzed by MicroED and GIWAXS was dPyr PDI because its structure had been determined previously by conventional single crystal XRD, and as such, this sample was appropriate for validating our experimental approach. dPyr PDI was synthesized following previously reported methods[9], and TEM grids were prepared by drop-casting from 10 mM toluene solutions (see Supporting Information). When the grids were imaged in the TEM, they were found to contain nanocrystalline material (Figure 1A). Crystallites that were well separated from other crystals and diffracted well (clear and sharp diffraction spots that extend to high-resolution) were used to collect continuous rotation MicroED data sets at 300 kV and a total dosage of approximately 5 e^{-}/Å^2 (see Supporting Information)[12]. It is important to note that the crystals used for MicroED were estimated to be on average 0.8 µm × 0.3 µm × 0.1 µm, which is approximately 4 ×10^4 times smaller in volume than what was initially used for X-ray structure determination by single crystal methods. Diffraction data extended to approximately 0.60 Å (Figure 1B). Diffraction data from three dPyr PDI crystallites were merged together for the final data set, and the structure was determined by direct methods. The MicroED structure of dPyr PDI (Figure 1C, D) is nearly identical to that determined by single crystal XRD with a Cc space group and deviations of 0.68%, 1.01%, 0.64%, and 0.55% between the MicroED and X-ray data sets for *a*, *b*, *c*, and *β*, respectively. Unlike the herringbone pattern commonly seen in the molecular packing of rylenes[7, 13], the packing in dPyr PDI is cofacial, asymmetric, and slip-stacked. This may be caused by steric crowding imposed by the pyrrolidine groups, which causes bowing and prevents the H-bonding between the imide groups that is typically seen in herringbone packing of rylenes.

GIWAXS data were collected on dPyr PDI films that were drop-casted onto glass slides to further corroborate the unit cell determined by MicroED, confirm the unit cell observed in the crystallites matches the packing in the films, and determine if they lie on the substrate with a preferred orientation. The scattering pattern is composed of well-defined, radially uniform rings, which indicates a crystalline sample with no preferential orientation with respect to the glass substrate (Figure 1E). dPyr PDI GIWAXS data was compared with the MicroED solved structures by generating a simulated dPyr PDI powder pattern of the MicroED structure using CrystalDiffract, and this pattern was then compared to the GIWAXS 1D integrated intensity versus *q* (Figure 1F). The two data sets are in good agreement, with all peaks on the simulated spectrum mapping onto peaks in the GIWAXS data. This match between MicroED and GIWAXS data confirms that the solved unit cell is what is prevalent in films and provides a pathway for identifying unit cell structure and orientation in device-related films.

Subsequently, MicroED was applied to solving the previously unknown crystal structure of dCN NDI, a naphthalene diimide, which is increasingly adopted in OFETs[7, 14] as an air-stable, n-type semiconductor because of its low lying LUMO[10, 15]. dCN NDI was synthesized following previously reported methods[10], and 10 mM toluene solutions were drop-casted directly onto TEM grids for MicroED interrogation (Figure S1). Crystallites of dCN NDI diffracted beyond 0.6 Å in some cases (Figure S2). Because dCN NDI crystals showed a preferred orientation on the grid, 8 crystals in total were merged to obtain a data set at 71.5% overall completeness at a resolution of 0.57 Å. Despite the relatively low completeness of the data, the

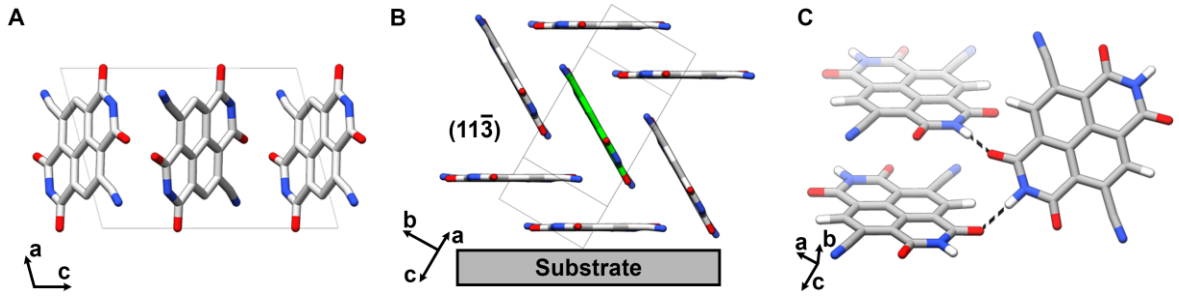

Figure 2. MicroED solved dCN NDI structure. Unit cell (box) perspective along (A) *b*-axis and (B) solved dCN NDI crystal structure, which shows herringbone packing, $P2_1/c$ space group, and a preferred (11$\bar{3}$) out-of-plane orientation with respect to the substrate. π-stacking, defined as the distance between molecular planes, is 3.20 Å and parallel or 60° with respect to the substrate. Single molecule of dCN NDI shown in green. (C) H-bonding between O and N–H on adjacent dCN NDI molecules are uniformly 1.85 Å and 175.15°. Atom colors: C, grey; N, blue; O, red; H, white. H have been omitted from (A) and (B) for clarity.

structure of dCN NDI was determined (R1/wR2 = 0.1690/0.3919), and it organized into a herringbone motif (Figure 2). The structure of the dCN NDI is arranged such that there are H-bonds formed between the carbonyl and amide groups of adjacent molecules (Figure 2C), such that each dCN NDI makes a total of 4 H-bonds with 4 other adjacent molecules. dCN NDI films for GIWAXS analysis were prepared on glass slides via thermal evaporation. Although drop casting of suspended dCN NDI crystallites gave satisfactory samples for TEM MicroED analysis, dCN NDI is not readily soluble in common organic solvents, so thermal evaporation was used to create smoother films with better GIWAXS resolution. Though different substrates and deposition methods were used, simulated powder data from the crystal structure matched well with the GIWAXS data (Figure S6). The X-ray scattering pattern (Figure S5) shows preferential out-of-plane orientation, perpendicular to the substrate, along the (11$\bar{3}$) plane and minor orientation along (100), (10$\bar{2}$), and (11$\bar{2}$). π-stacking in dCN NDI occurs either parallel or 60° to the substrate (Figure 2B).

The third compound that we analyzed, dDPP, whose crystal structure has not been previously determined, was studied because it has been shown to undergo singlet fission (SF) with high yields and lifetimes in films.[8] SF is highly influenced by packing geometry[16], and in our previous study the lack of a crystal structure impeded our ability to correlate SF yields and lifetimes to solid state packing. dDPP possesses a diketopyrrolopyrrole core, chiral alkyl side chains extending off the core Ns, and diamidopyridine (DAP) moieties added to provide H-bonding to adjacent molecules. For dDPP, MicroED data from 7 crystals were collected and merged together to produce a final refined structure at 0.90 Å (Figure 3A) with a $P2_1/n$ point group. In the solved crystal structure, H-bonding between neighboring dDPPs occurs between only one of the amide groups of the DAP substituents (Figure 3B), a supramolecular interaction we have observed previously[17]. The DAP•••DAP H-bonding arrangement in dDPP has similar H-bond angles and distances as in the previously reported structure of mDPP, which contains one DAP group instead of two, and whose crystal structure has been previously solved using conventional single crystal methods.[17]

dDPP films for GIWAXS analysis were prepared on glass slides via drop-casting from 10 mM toluene solutions. The scattering pattern (Figure S5) shows preferential out-of-plane orientation along the (011) (Figure 3A), (012), and (013) planes, which orient close together. This geometry places the *a*-axis, the direction of π-stacking, in a preferred orientation that is parallel to the substrate. Though dDPP GIWAXS data and powder pattern generated from MicroED unit cells possess similar shape (Figure S6), the first and third major peaks of the simulated pattern are shifted slightly toward larger 2ϑ, whereas the second major peak of the simulated data is in very good agreement with the GIWAXS pattern. The first peak in the simulated pattern is actually composed of two overlapping peaks, which correspond to (002) and (011). The second and third peaks in the simulated data correspond to (012) and (013), respectively. Because the subtle mismatches between the simulated MicroED powder patterns and the GIWAXS data are all in 0*kl*, we hypothesize that there is some variation in the *b* and *c* axes of the crystals in films deposited on glass substrates compared to crystallites deposited on continuous carbon TEM grids, and these differences may be caused by interactions with the substrate during crystallization. This is reasonable considering the *a*-axis falls along the dDPP π stacking direction and is likely invariant, while *b* and *c* axes may vary because of different possible packing arrangements along the flexible alkyl chains (Figure S3C and D). Because peaks where *h* is non-zero are not prominent in either the simulated MicroED powder or the GIWAXS data, we are unable to independently determine the nature of any changes in the packing along the *a*-axis. This highlights an important caveat to MicroED and all single crystal XRD methods, which is that typically only the best diffracting crystals are chosen for data collection and further analysis, though they may represent just one of multiple polymorphs in a sample; therefore, care must be taken to investigate many crystallites to build more reliable data sets. This demonstrates the importance of combining other methods with MicroED, such as GIWAXS, as we have done here, to understand film packing.

In conclusion, MicroED was used to determine structures from nanocrystalline organic semiconductors, circumventing the need to grow larger crystals for X-ray diffraction studies. MicroED can be a valuable tool when used in combination with GIWAXS to construct a 3D representation of packing within films. In the case of both dPyr PDI and dCN NDI, the packing in

crystallites and films matched well. dDPP possessed a slight mismatch, which teaches us that care that must be taken when correlating crystals and films. Future investigations will involve absolute structure determination through modeling dynamic scattering[18] and multicomponent supramolecular crystals[8, 17]. With continued development, the application of electron diffraction methods, particularly in combination with GIWAXS, promises to become even more powerful and ubiquitous tool for organic and materials chemistry.

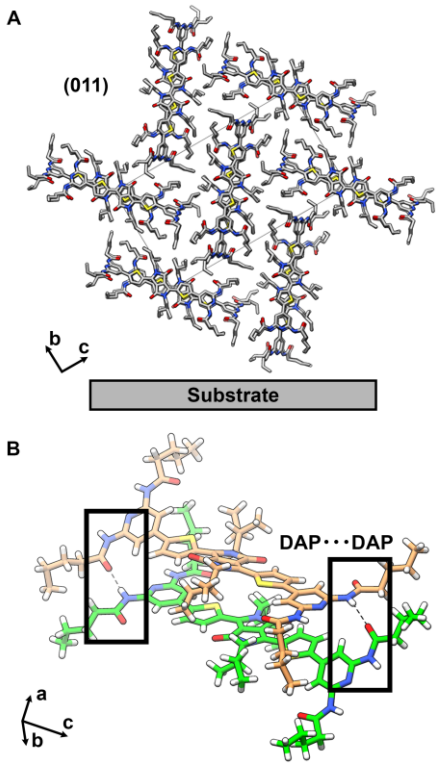

Figure 3. (A) MicroED solved dDPP of $P2_1/n$, unit cell structure shown in grey box, and one of the preferred (011) out-of-plane orientations with respect to the substrate. (B) H-bonding between DAP groups of adjacent, asymmetric DPP molecules (shown as dotted line) are 2.20 Å and 156.74° or 1.98 Å and 169.60°, π-stacking distances are 3.55 Å (top molecule in asymmetric unit with molecule above), 3.66 Å (two molecules in asymmetric unit), and 3.36 Å (bottom molecule in asymmetric unit with molecule below). Single molecule of dDPP shown in green, atom colors: C, grey; N, blue; O, red; H, white.

AL thanks the NSF CREST Center for Interface Design and Engineered Assembly of Low Dimensional systems (IDEALS), NSF grant number HRD1547830. AB and BLN thank the Air Force Office of Scientific Research (FA9550-19-1-0220 and FA9550-18-1–0012, respectively). AB also thanks NSF CHE, grant number CHE-1610755. We thank Marc Messerschmidt, Michael Martynowycz and Tim Gruene for helpful discussions on electron diffraction data processing and refinement. We acknowledge the use of the Titan Krios within the Eyring Materials Center at Arizona State University and for NSF grant 1531991 for the funding of this instrument. This research used beamline 12-ID SMI of the National Synchrotron Light Source II (NSLS-II) and the Center for Functional Nanomaterials (CFN), both of which are U.S. Department of Energy (DOE) Office of Science User Facilities operated for the DOE Office of Science by Brookhaven National Laboratory under Contract No. DE-SC0012704. We thank Guillaume Freychet and Mikhail Zhernenkov for their assistance performing experiments at the beamline.

Conflicts of interest

There are no conflicts to declare

Notes and references

1. C. Wang, H. Dong, L. Jiang and W. Hu, *Chem. Soc. Rev.*, 2018, **47**, 422-500; A. F. Paterson, S. Singh, K. J. Fallon, T. Hodsden, Y. Han, B. C. Schroeder, H. Bronstein, M. Heeney, I. McCulloch and T. D. Anthopoulos, *Adv. Mater.*, 2018, **30**, 1801079; F. Yang, S. Cheng, X. Zhang, X. Ren, R. Li, H. Dong and W. Hu, *Adv. Mater.*, 2018, **30**, 1702415.
2. J. Hou, O. Inganäs, R. H. Friend and F. Gao, *Nat. Mater.*, 2018, **17**, 119-128; P. Cheng, G. Li, X. Zhan and Y. Yang, *Nat. Photonics*, 2018, **12**, 131-142; J. Zhang, H. S. Tan, X. Guo, A. Facchetti and H. Yan, *Nat. Energy*, 2018, **3**, 720-731.
3. A. M. Levine, S. Biswas and A. B. Braunschweig, *Nanoscale Adv.*, 2019, **1**, 3858-3869; X. Guo, N. Zhou, S. J. Lou, J. Smith, D. B. Tice, J. W. Hennek, R. P. Ortiz, J. T. L. Navarrete, S. Li, J. Strzalka, L. X. Chen, R. P. H. Chang, A. Facchetti and T. J. Marks, *Nat. Photonics*, 2013, **7**, 825-833; F. Zhao, C. Wang and X. Zhan, *Adv. Energy Mater.*, 2018, **8**, 1703147.
4. B. L. Nannenga and T. Gonen, *Nat. Methods*, 2019, **16**, 369-379; B. L. Nannenga, D. Shi, J. Hattne, F. E. Reyes and T. Gonen, *eLife*, 2014, **3**, e03600; D. Shi, B. L. Nannenga, M. G. Iadanza and T. Gonen, *eLife*, 2013, **2**, e01345.
5. T. Gruene, J. T. C. Wennmacher, C. Zaubitzer, J. J. Holstein, J. Heidler, A. Fecteau-Lefebvre, S. De Carlo, E. Muller, K. N. Goldie, I. Regeni, T. Li, G. Santiso-Quinones, G. Steinfeld, S. Handschin, E. van Genderen, J. A. van Bokhoven, G. H. Clever and R. Pantelic, *Angew. Chem. Int. Ed.*, 2018, **57**, 16313-16317; C. G. Jones, M. W. Martynowycz, J. Hattne, T. J. Fulton, B. M. Stoltz, J. A. Rodriguez, H. M. Nelson and T. Gonen, *ACS Cent. Sci.*, 2018, **4**, 1587-1592.
6. J. Feng, W. Jiang and Z. Wang, *Chem.: Asian J.*, 2018, **13**, 20-30; W. Jiang, Y. Li and Z. Wang, *Acc. Chem. Res.*, 2014, **47**, 3135-3147; S. W. Eaton, L. E. Shoer, S. D. Karlen, S. M. Dyar, E. A. Margulies, B. S. Veldkamp, C. Ramanan, D. A. Hartzler, S. Savikhin, T. J. Marks and M. R. Wasielewski, *J. Am. Chem. Soc.*, 2013, **135**, 14701-14712.
7. X. Zhan, A. Facchetti, S. Barlow, T. J. Marks, M. A. Ratner, M. R. Wasielewski and S. R. Marder, *Adv. Mater.*, 2011, **23**, 268-284.
8. A. M. Levine, C. Schierl, B. S. Basel, M. Ahmed, B. A. Camargo, D. M. Guldi and A. B. Braunschweig, *J. Phys. Chem. C*, 2019, **123**, 1587-1595.
9. L. M. Smieska, Z. Li, D. Ley, A. B. Braunschweig and J. A. Marohn, *Chem. Mater.*, 2016, **28**, 813-820.
10. G. S. Vadehra, R. P. Maloney, M. A. Garcia-Garibay and B. Dunn, *Chem. Mater.*, 2014, **26**, 7151-7157.
11. W. Li, K. H. Hendriks, M. M. Wienk and R. A. J. Janssen, *Acc. Chem. Res.*, 2016, **49**, 78-85; C. B. Nielsen, M. Turbiez and I. McCulloch, *Adv. Mater.*, 2013, **25**, 1859-1880; Y. Wu and W. Zhu, *Chem. Soc. Rev.*, 2013, **42**, 2039-2058.
12. B. L. Nannenga, D. Shi, A. G. Leslie and T. Gonen, *Nat Methods*, 2014, **11**, 927-930.
13. K. C. See, C. Landis, A. Sarjeant and H. E. Katz, *Chem. Mater.*, 2008, **20**, 3609-3616.

14. S. V. Bhosale, C. H. Jani and S. J. Langford, *Chem. Soc. Rev.*, 2008, **37**, 331-342.
15. J. Chang, Q. Ye, K.-W. Huang, J. Zhang, Z.-K. Chen, J. Wu and C. Chi, *Org. Lett.*, 2012, **14**, 2964-2967.
16. M. B. Smith and J. Michl, *Annu. Rev. Phys. Chem.*, 2013, **64**, 361-386; E. Busby, J. Xia, Q. Wu, J. Z. Low, R. Song, J. R. Miller, X. Y. Zhu, Luis M. Campos and M. Y. Sfeir, *Nat. Mater.*, 2015, **14**, 426–433; S. N. Sanders, A. B. Pun, K. R. Parenti, E. Kumarasamy, L. M. Yablon, M. Y. Sfeir and L. M. Campos, *Chem*, 2019, **5**, 1988-2005.
17. C. X. Guzman, R. M. K. Calderon, Z. Li, S. Yamazaki, S. R. Peurifoy, C. Guo, S. K. Davidowski, M. M. A. Mazza, X. Han, G. Holland, A. M. Scott and A. B. Braunschweig, *J. Phys. Chem. C*, 2015, **119**, 19584-19589.
18. P. Brázda, L. Palatinus and M. Babor, *Science*, 2019, **364**, 667-669.